Mass and heat transfer between evaporation and condensation surfaces: Atomistic simulation and solution of Boltzmann kinetic equation

Article *in* Proceedings of the National Academy of Sciences · April 2018

DOI: 10.1073/pnas.1714503115

CITATIONS
0

READS
90

5 authors, including:

Vasily Zhakhovsky
All-Russia Research Institute of Automatics (VNIIA)
194 PUBLICATIONS **1,788** CITATIONS
SEE PROFILE

Alexei Pavlovich Kryukov
Moscow Power Engineering Institute (Technical University)
80 PUBLICATIONS **488** CITATIONS
SEE PROFILE

Vladimir Yu. Levashov
Institute of Mechanics of Lomonosov Moscow State University, Ru...
37 PUBLICATIONS **253** CITATIONS
SEE PROFILE

I. N. Shishkova
Moscow Power Engineering Institute (Technical University)
44 PUBLICATIONS **227** CITATIONS
SEE PROFILE

SPECIAL FEATURE: PERSPECTIVE

Mass and heat transfer between evaporation and condensation surfaces: Atomistic simulation and solution of Boltzmann kinetic equation

Vasily V. Zhakhovsky (Василий Жаховский)[a,1], Alexei P. Kryukov[b], Vladimir Yu. Levashov[b,c], Irina N. Shishkova[b], and Sergey I. Anisimov[d]

Edited by William A. Goddard III, California Institute of Technology, Pasadena, CA, and approved March 21, 2018 (received for review December 25, 2017)

Boundary conditions required for numerical solution of the Boltzmann kinetic equation (BKE) for mass/heat transfer between evaporation and condensation surfaces are analyzed by comparison of BKE results with molecular dynamics (MD) simulations. Lennard–Jones potential with parameters corresponding to solid argon is used to simulate evaporation from the hot side, nonequilibrium vapor flow with a Knudsen number of about 0.02, and condensation on the cold side of the condensed phase. The equilibrium density of vapor obtained in MD simulation of phase coexistence is used in BKE calculations for consistency of BKE results with MD data. The collision cross-section is also adjusted to provide a thermal flux in vapor identical to that in MD. Our MD simulations of evaporation toward a nonreflective absorbing boundary show that the velocity distribution function (VDF) of evaporated atoms has the nearly semi-Maxwellian shape because the binding energy of atoms evaporated from the interphase layer between bulk phase and vapor is much smaller than the cohesive energy in the condensed phase. Indeed, the calculated temperature and density profiles within the interphase layer indicate that the averaged kinetic energy of atoms remains near-constant with decreasing density almost until the interphase edge. Using consistent BKE and MD methods, the profiles of gas density, mass velocity, and temperatures together with VDFs in a gap of many mean free paths between the evaporation and condensation surfaces are obtained and compared. We demonstrate that the best fit of BKE results with MD simulations can be achieved with the evaporation and condensation coefficients both close to unity.

evaporation | condensation | Boltzmann kinetic equation | molecular dynamics

Evaporation and condensation can be realized in different natural phenomena and technologies. A peculiarity of these processes is the coupled mass and heat transfer from evaporation to condensation surface. Nowadays, a correct description of the transport processes across the interfacial surfaces is required for the development of new advanced technologies and solution of the known engineering problems. Among them, the problem of removing heat from space vehicles, developing technologies based on the interaction of matter in the form of cryogenic corpuscular targets with high-energy beams, evaporation of droplets on superhydrophobic surfaces using liquid droplets as the molecular concentrators of ultradilute solutions, the development of effective vacuum drying methods—all of these tasks are inextricably linked with the solution of the evaporation–condensation problem.

The main goal in considering the coupled mass/heat transfer is an accurate evaluation of the masses of evaporated or condensed material. Determination of these quantities is important because a significant heat can be diverted from the interfacial surface, which, as a consequence, leads to cooling of the condensed phase. For example, when considering the evaporation of a liquid droplet placed in a steam–gas mixture, the inaccuracies in calculating the evaporation rate can lead to

[a]Center for Fundamental and Applied Research, Dukhov Research Institute of Automatics, Moscow 127055, Russia; [b]Department of Low Temperatures, Moscow Power Engineering Institute, Moscow 111250, Russia; [c]Institute of Mechanics, Lomonosov Moscow State University, Moscow 119192, Russia; and [d]Landau Institute for Theoretical Physics, Russian Academy of Science, Chernogolovka 142432, Russia

Author contributions: S.I.A. designed research; V.V.Z., A.P.K., V.Y.L., and I.N.S. performed research; V.V.Z., A.P.K., V.Y.L., and S.I.A. analyzed data; and V.V.Z., A.P.K., and V.Y.L. wrote the paper.

The authors declare no conflict of interest.

This article is a PNAS Direct Submission.

[1]To whom correspondence should be addressed. Email: 6asi1z@gmail.com.

This article contains supporting information online at www.pnas.org/lookup/suppl/doi:10.1073/pnas.1714503115/-/DCSupplemental.

errors in determining the pattern of temperature changes at the interfacial surface, which may result in inaccurate forecasts of the droplet temperature and a complete evaporation time.

As noted in ref. 1, despite the simplicity of the formulation of the evaporation–condensation problem, its solution encounters certain difficulties in the general case. Traditionally, it is assumed that the heat coming to the interphase boundary is spent on evaporation and heating of the particles, and the resulting vapor is diverted from the evaporation surface by diffusion. It is believed that the concentration of the evaporated gas near the interphase boundary is equal to the equilibrium vapor concentration. This assumption was first used in ref. 2 to consider evaporation of a spherical drop. However, this is not the case, since the vapor near the interfacial surface will be saturated only if a diffusion rate of gas escape is lower than an arrival rate of molecules from the interphase boundary. Ref. 3 showed the existence of a concentration jump near the interphase boundary. One of the refinements of the evaporation–condensation theory can be achieved by invoking the kinetics of interaction of vapor molecules with the surface of the liquid phase and also with each other. In refs. 4 and 5, using the methods of molecular–kinetic theory, a mass flux of evaporated molecules was evaluated. A disadvantage of the formula proposed in these papers lies in the fact that it was obtained for a free molecular flow of the evaporated gas—that is, for the conditions where emitted particles do not interact with molecules presented near the surface.

The next stage in the study of evaporation–condensation dates back to the 1960s, when the dynamics of rarefied gases was developed rapidly. The needs of technology development led to the emergence of more rigorous calculation techniques based on the exact or approximate solution of the Boltzmann kinetic equation (BKE). A linear theory was being formulated at this time. The beginning was laid by the work in ref. 6, in which the form of the velocity distribution function (VDF) near the interphase boundary was adopted rather than in the derivation of the Hertz–Knudsen formula (4, 5). The authors suggested that the VDF for molecules moving to this boundary is the same as for a negative half-space of velocities at a considerable distance from the interface of the phases. Then, by writing down the expression for the mass flow from definition, they obtained a result that was two times different from the mass flow calculated by the Hertz–Knudsen formula.

Linearized, or more simply a linear theory of, evaporation and condensation was developed by Labuntsov and Muratova in refs. 7 and 8. At about the same time, many researchers (9–16) and Anisimov et al. (17–19) were focused on the solution of nonlinear evaporation–condensation problems with the use of the kinetic theory of gases.

With the advancement of computers, the direct numerical solution of the BKE began to be applied to the evaporation–condensation problems (20–24). For solving the BKE, it is necessary to specify the correct boundary conditions for the VDFs of evaporated and condensed molecules. The shapes of VDFs together with the evaporation and condensation coefficients, determining the corresponding fluxes through the evaporation and condensation surfaces, are involved in those boundary conditions. In the previously listed works, a semi-Maxwellian VDF with zero transport velocity was taken as such a function. However, as noted in ref. 25, "no serious theoretical conclusion of such a boundary condition is known to us."

The measured evaporation and condensation coefficients may vary greatly from experiment to experiment. The condensation coefficient for water ranges from ~0.01 to 1 as noted in the review (26). It seems likely that such a wide spread can be explained by the fact that those coefficients were measured not at the interface but over a distance of many mean free paths in the vapor. Moreover, even the small differences between the experimental conditions (such as chemical impurities on the interface and variation of surface temperatures of liquids being investigated) may have a dramatic effect on the measurement results. The dependence of evaporation and condensation coefficients from the surface temperature is also reported in simulation works (27, 28). It was found that those coefficients, which are close to unity at low temperatures, begin to decrease if the surface temperature is increased well above the triple point.

It should be noted that the molecular–kinetic approach allows us to correctly describe the change in the macroparameters of the vapor/gas near the interfacial surface, but it is assumed that the state of the condensed phase remains unchanged. On the other hand, the VDF of molecules escaping from the surface can be affected by processes occurring near this surface, both from the liquid side and from the vapor side. In this connection, the approach in which both the condensed and vapor phases are considered within the framework of a single modeling method is obvious. As a research method, the molecular dynamics (MD) simulation has been widely used presently. There are several known works in which the calculation of the VDF of molecules emitted from the interphase boundary layer is performed by the MD method (25, 29–31) and the analysis of the simulation results lead to the conclusion about the proximity of the VDF of vapor molecules "flying" from the interphase to the Maxwellian distribution.

In refs. 28 and 32, the problem of recondensation through a small vapor gap with the thickness of about 7 nm, which leads to a Knudsen flow with $Kn \sim 1$ roughly, is investigated via MD simulation and by the solution of the Enskog–Vlasov equation with the Direct Simulation Monte Carlo (DSMC) method. The authors came to the following conclusion: "On the basis of the results of this study, we constructed the kinetic boundary conditions (KBC) for the hard-sphere molecules in consideration of the liquid temperature dependence in the course of a steady net evaporation and condensation; however, the application of the KBC during unsteady net evaporation-condensation is extremely important." Furthermore, the same two-surface method used in refs. 28 and 32 was applied in ref. 33 to study the evaporation–condensation in an unsteady transient regime on a short MD time scale. The authors of ref. 34 noted that there is a deviation from the Maxwellian VDF for particles flying in the direction normal to the interfacial surface: "However, the detailed mechanism of the deviation has not been clarified yet."

Numerous papers using the MD method indicate that an important question in determining the KBC is at which position of the boundary between the liquid and gas phases those KBC should be determined (27, 32, 34, 35). The authors of ref. 35 discuss the influence of the KBC position on the mass flow of the evaporating substance.

It seems obvious the way in which a joint (cross-linked) version of the description is used. That is, the liquid phase and the region near the interphase boundary layer are described by the MD method, next the methods of the kinetic theory of gases are used, and finally the continuum mechanics approaches are applied on distances larger than the 10 to 20 mean free paths. However, such attempts are faced with certain problems and difficulties. The characteristic time scale of the MD processes and the kinetic relaxation time differ approximately by a factor of 10^4. Therefore, more than 10^5 simulation steps must be taken to trace the behavior of an atomic system during the average interatomic collision time. The MD method deals with the coordinates and velocities of the particles, but for a molecular–kinetic approach, "this description of the motion of

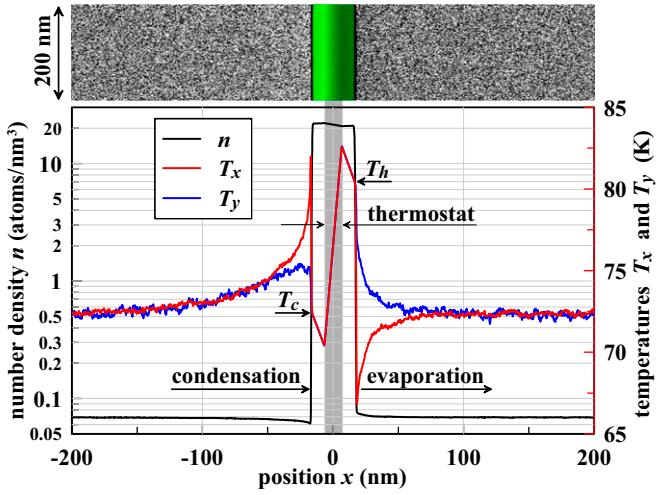

Fig. 1. MD computational domain for evaporation from the right hot side of liquid film and condensation on the left cold side of the same film placed in periodical conditions. Profiles of atom number density, longitudinal T_x, and transverse T_y temperatures are taken from MD simulation providing $T_c = 72.3$ for a cold surface and $T_h = 80.4$K for a hot one. The Langevin thermostat maintains a required temperature gradient for atoms in a gray zone $x_i \in [-7,7\text{nm}]$ inside the film with a thickness of 32.7nm. The thermostat also keeps the mass center of film at rest by adjusting the mass flow velocity from the cold to the hot side. Here this flow velocity is $\approx u_x = 0.129\text{m/s}$ at the $x = 0$. See details in Fig. S1.

the gas is unnecessarily complete. Therefore, we must resort to a less complete statistical description of the behavior of the system" as a note in ref. 36. Also, the results of molecular–kinetic calculations in the form of VDF cannot be used to obtain information on the particle coordinates and velocities necessary for MD simulation. Accordingly, the mutual exchange of results of calculations obtained by molecular–kinetic and MD methods becomes problematic.

In this work, a nonequilibrium vapor flow from the evaporation to condensation boundary layer is considered in detail on an atomic scale using the MD method, which provides the classical trajectories of interacting atoms starting from a hot bulk material and reaching a cold material after traveling through a gas gap. To simplify the modeling of gas flow, the exact atom positions $\mathbf{r}_i$ and velocities $\mathbf{v}_i$ can be replaced by a probability density function $f(\mathbf{r}, \mathbf{v}, t)$ to find dN molecules having positions near $\mathbf{r}$ and velocities near $\mathbf{v}$ within a phase-space volume $d\mathbf{r}d\mathbf{v}$ at time t such as $dN = f(\mathbf{r}, \mathbf{v}, t)d\mathbf{r}d\mathbf{v}$. Upon integrating $f(\mathbf{r}, \mathbf{v}, t)$, also called a distribution function, over a whole range of velocity, we obtain a local number density $n(\mathbf{r}, t)$ of molecules. In a volume with spatially uniform distribution of molecules, a VDF $F(\mathbf{v}, t)$ can be obtained by integrating $f(\mathbf{r}, \mathbf{v}, t)d\mathbf{r}$ over the volume.

The BKE (36) describing evolution of the $f(\mathbf{r}, \mathbf{v}, t)$ at the absence of external forces is given by

$$\frac{\partial f}{\partial t} + \mathbf{v}\frac{\partial f}{\partial \mathbf{r}} = I, \qquad [1]$$

where $\mathbf{r}(x, y, z)$ are Cartesian coordinates, $\mathbf{v}(v_x, v_y, v_z)$ is the molecule velocity in a laboratory coordinate system at time t, and I is a collision integral. The different forms of the collisional integral are considered in refs. 20 and 21. Here in this work, the simplest form for the hard sphere collisions is used.

Our prime goal is to make a bridge from atomistic simulation to a probabilistic approach through a more penetrating insight into the atomic-scale mechanism of evaporation and condensation, which determines the VDFs at the corresponding interfaces. We performed the large-scale MD simulations to find the best boundary conditions, including their positions, evaporation and condensation coefficients, and the shapes of VDFs, which can be used in the solution of BKE providing the best agreement with data obtained from the MD simulations. For consistency of BKE with MD results, the saturated vapor density and transport cross-section were precomputed by MD and then used in the BKE method.

Simulation Techniques

Equilibrium evaporation and condensation processes take place in an interphase transition layer between the coexisting condensed phase and its vapor. For MD simulation of nonequilibrium evaporation–condensation, the two surfaces of condensed phase at different temperatures are required. This condition can be complied with using both sides of a single film as illustrated in Fig. 1, where the condensed phase of argon is placed in the middle of the MD computational domain. Periodical boundary conditions are imposed on all three dimensions of the domain, which has typical dimensions of $L_x = 400$nm and $L_y = L_z = 200$nm. The total number of atoms was about 29.15 million in our MD simulations of evaporation–condensation.

To establish both evaporation and condensation processes in a single simulation, a temperature gradient is maintained by the Langevin thermostat with target temperature $T(x)$ depending on atom position in the film. The thermostat is only applied to atoms moving in a gray zone nearby the center of film as shown in Fig. 1; thus, the interphase layers between the condensed phase and vapor are not acted upon by the thermostat forces. The Langevin forces are given by

$$m_i d\vec{v}_i/dt = \vec{\xi}_i - \gamma\left(\vec{v}_i - \tilde{u}_x\right), \qquad [2]$$

where the force acting on each atom i is a sum of a Gaussian-distributed random force $\vec{\xi}_i$ and a frictional damping term (37). The last is determined by a friction coefficient γ and a thermal velocity of atom in reference to a target flow velocity $\tilde{u}_x$. To reproduce the temperature gradient within the film, the dispersion $\langle\xi^2\rangle$ of random forces and the friction coefficient must satisfy the condition $\langle\xi^2\rangle\Delta t/2\gamma = T(x)$, where Δt is an MD simulation time step. Then, the dispersion becomes a function of

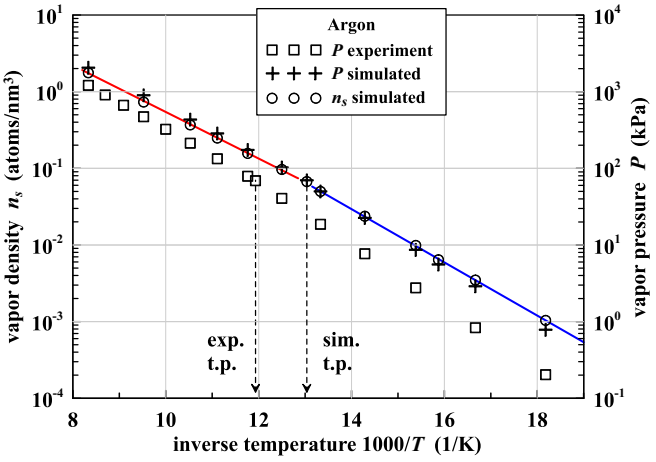

Fig. 2. Pressure and atom number density n_s of saturated vapor in equilibrium with the condensed phase of argon. Red line fitted to the vapor density in the liquid–vapor system and the blue line fitted to the vapor density in the solid–vapor system are used for estimating vapor density between data points. The experimental data from ref. 38, pp 6-128 and 15-10. The triple point of simulated argon $T_{t.p.} = 76.7$K is lower than the experimental $T_{t.p.} = 83.8058$K.

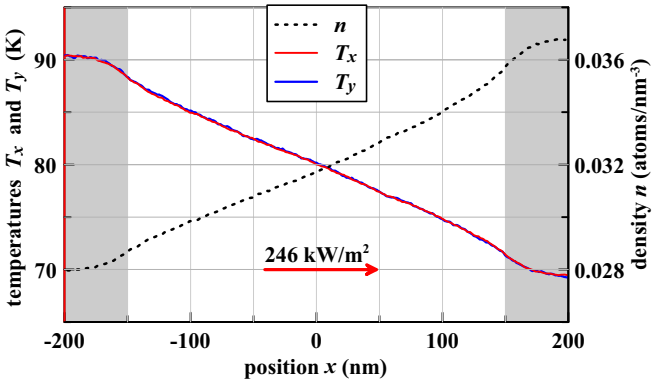

Fig. 3. MD simulation of steady heat flux from the left heating thermostat with $T_h = 90$K to the right cooling thermostat with $T_c = 70$K applied in the gray zones. A transport cross-section for BKE is fitted to get the same heat flux of 246kW/m² produced by the temperature gradient of 0.05K/nm imposed at $x = 0$.

atom position x_i because the friction coefficient is set to a constant in our MD simulation.

To maintain the steady positive atom flux across the MD domain and keep the film at rest, the Langevin target velocity $\tilde{u}_x$ is coupled with a displacement of film mass center using a negative feedback control. After reaching the stationary regime of vapor flow, such feedback control provides almost a fixed position of the film with negligible irregular fluctuations of mass center in the range less than ±0.01nm, which is much smaller than a thickness of the interphase layer of ~2nm for liquid argon at $T = 80$K. For steady evaporation–condensation, the atom flux in direction x is a constant everywhere regardless of local density. As a result, the mass velocity at the center of the film is less than gas flow speed by a factor equal to a density ratio between condensed phase and vapor. In the simulation shown in Fig. 1, the vapor mass velocity is about 40m/s in the middle of the gap between evaporation and condensation surfaces, while the liquid flows with 0.129m/s near the center of film, with the thickness of 32.7nm defined as a distance between positions of hot and cold surfaces having temperatures T_h and T_c, respectively. Determination of surface positions is discussed in *Evaporation Coefficient from MD Simulation*. The detailed profiles of target temperature and flow variables in the film and surrounding vapor are presented in *SI Appendix*.

MD simulations were performed with a smoothed Lennard–Jones (L–J) potential (39) given by

$$\phi(r) = 4\varepsilon\left[(\sigma/r)^{12} - (\sigma/r)^{6}\right] + a_2x^2 - a_3x^3, \qquad [3]$$

where r is an interatomic distance and $x = (r/\sigma)^2 - (r_0/\sigma)^2$. The coefficients $\varepsilon = 1.0312$kJ/mol, $\sigma = 0.33841$nm, $a_2 = 1.3647 \times 10^{-4}$kJ/mol, and $a_3 = 2.4614 \times 10^{-4}$kJ/mol are fitted to reproduce argon fcc crystal at zero temperature, which has the lattice parameter of 0.524673 nm and the cohesive energy of 7.74005 kJ/mol. The position of the potential minimum $r_0 = 2^{1/6}\sigma$ is identical to that in the original L–J potential. The smoothing coefficients a_2 and a_3 were chosen to satisfy the conditions $\phi(r_c) = 0$ and $\phi'(r_c) = 0$ at the cutoff radius $r_c = 0.8125$nm.

A density of vapor in equilibrium with the condensed phase is required to run the BKE calculation of evaporation and condensation because the density $n_s(T)$ of saturated vapor is used to set a boundary condition for VDF. Using the smoothed L-J potential Eq. **3** the vapor pressure and atom number density are evaluated in several MD simulations of equilibrium liquid-vapor and solid-vapor systems. Fig. 2 shows the calculated and experimental values for argon. The visible difference in vapor pressure indicates that the smoothed L–J potential, fitted to the experimental parameters of solid Ar, overestimates the pressure. Using the phase-coexistence MD method, we obtained all three phases in equilibrium at the triple point $T_{t.p.} = 76.7$K of simulated argon, which is appreciably lower than the experimental triple point $T_{t.p.} = 83.8058$K (38).

Numerical solution of BKE of the evaporation–condensation problem is performed only for vapor gaps between two interfaces defined from MD simulated profiles as the outer boundaries of interphase transition layers from the bulk condensed phase to vapor. While the results of BKE calculations are almost insensitive to the delimitation of interfaces, they depend highly on the definition of interface temperatures. Those temperatures are also evaluated from MD simulated profiles at some position inside the transition layer. The interface definitions are introduced in the next section.

With the vapor density function, positions of interfaces, and their temperatures provided by MD simulations, the BKE Eq. **1** can be solved numerically in the vapor gap. We use a finite-difference computational method described in refs. 20, 21, and 40, in which a spherical velocity domain is represented by a discrete 3D mesh of velocity nodes. The discretized BKE equation for each node is solved in two steps. First, the spatial displacements are calculated without collisions, and the Courant condition used for a time step Δt guarantees that even fastest nodes cannot move more than one spatial step Δx. Then the collisions are calculated and taken into account.

The collisional integral is evaluated by the quasi Monte Carlo method using the Korobov's pseudorandom sequences (21). For simplicity, the interatomic collision of L–J atoms is considered as a collision between hard spheres of diameter d. The last is an adjustable parameter that must be determined from MD simulation for consistency between BKE and MD methods. The collision cross-section determined by the diameter d is adjusted to provide a steady heat flux close to that derived from

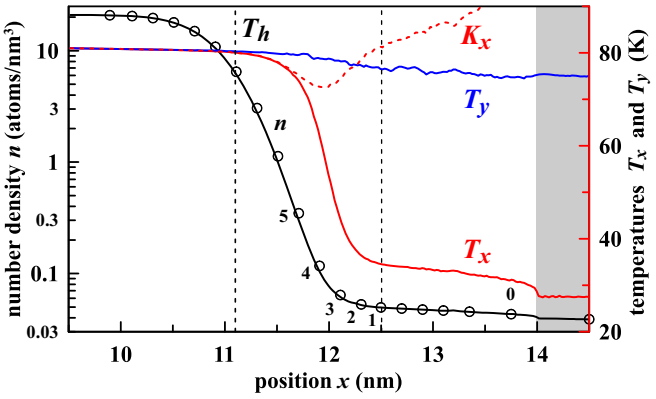

Fig. 4. Number density and temperatures profiles in a hot interphase layer and a small vapor gap $l_{gap} = 1.5$nm bounded by the Maxwell demon. The left boundary of the nonequilibrium part of the interphase layer (the left vertical dashed line) is determined by a point of divergence between longitudinal T_x and transverse T_y temperatures. This point is used for definition of the surface temperature T_h. The right boundary (the right dashed line) corresponds to a point where density and T_x starts to decrease linearly. The Maxwell demon ensures that all atoms in the gray zone have $v_x > 0$. Numbers along the density profile indicate positions where velocity data for VDFs are gathered. Atoms pass the interphase almost without loss of their longitudinal component of kinetic energy K_x expressed in the temperature units.

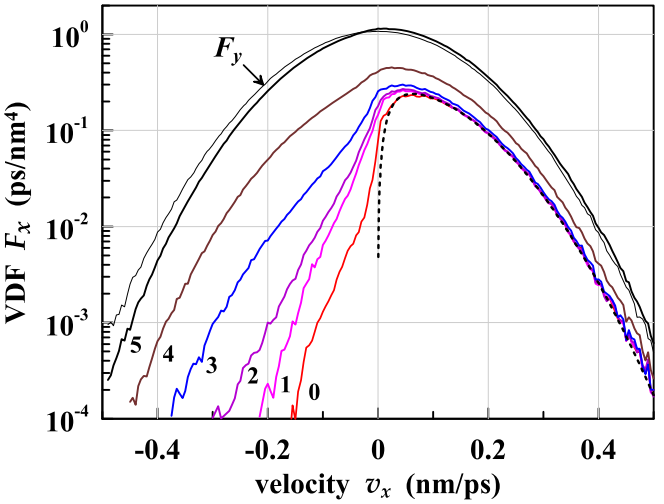

Fig. 5. Evolution of VDFs within the nonequilibrium part of the interphase layer. Numbers indicate positions in the layer shown in Fig. 4. The thin black line shows VDF for transverse velocity v_y. The last VDF at the edge of the interphase layer is marked by 1, while VDF in vapor is marked by 0. Dashed line shows a model vapor VDF from Eq. 4 with $\varepsilon_b = 0.025$kJ/mol. Major changes in VDF take place in the interphase layer.

MD simulation of heat transfer between hot and cold zones of gas gap shown in Fig. 3. L–J atoms within the left hot and right cold zones in the MD domain with a rigid wall at ±200 nm are subjected to two Langevin thermostats supporting 90K and 70K, respectively. Initially atoms were placed in the domain at a constant density of $n = 0.032\text{nm}^{-3}$. After reaching a steady regime, the heat flux, the number density, and temperature gradient were measured at the center $x = 0$. Using those MD data, the cross-section was found to equal $d = 0.55$nm to reproduce the almost identical heat flux of 245kW/m^2 in BKE calculations.

For the vapor density $n = 0.0963\text{nm}^{-3}$ in equilibrium with L–J liquid at $T = 80$K, a mean free path in a hard sphere system is $\lambda = 1/\sqrt{2}n\pi d^2 = 7.73$ nm, which gives the Knudsen number $\text{Kn} = \lambda/L_{gap} = 0.021$ for the vapor gap length of $L_{gap} = 364.3$nm shown in Fig. 1.

To obtain evaporation and condensation coefficients, which are the basic parameters governing the boundary conditions in the BKE method, we use the flow profiles and VDFs gained from atomistic trajectories simulated by the MD method. The most appropriated coefficients can be found via comparison of VDFs from numerical solution of BKE with VDFs obtained from the MD simulation. The VDFs in a steady vapor flow at x positions are calculated as $F(x, v_x, t) = \int dydz \int dv_y dv_z f(\mathbf{r}, \mathbf{v}, t)$. For steady flow, the distributions are independent of time, which allows us to accumulate atom position and velocity statistics during MD simulation. Further integration over v_x gives an atom number density profile $n(x) = \int dv_x F(x, v_x)$.

The steady profiles of density, mass flow velocity, and temperature are obtained by averaging the corresponding values in spatial slabs with the small thickness of 0.02nm along the x–axis and during the entire time of productive MD simulation, which is performed after the attainment of a steady regime. The profile of flow velocity $u_x(x) = \langle v_x \rangle$, the longitudinal $T_x(x) = \frac{m}{k_B}\langle (v_x - u_x)^2 \rangle$, and transverse $T_y(x) = \frac{m}{2k_B}\langle v_y^2 + v_z^2 \rangle$ temperatures are calculated from the corresponding components of atom velocities v_x, v_y, and v_z.

Evaporation Coefficient from MD Simulation

The transition of atoms from bulk phase to vapor can be imagined as a jump over a potential barrier with the height equal to the atom binding energy ε_b in the condensed phase. It is assumed in this naive model that the barrier is infinitely thin and an atom should spend its kinetic energy to overcome the barrier. As a result, the atoms with kinetic energy ε_l in direction x toward the vapor exceeding the binding energy $\varepsilon_l > \varepsilon_b$ can go to the vapor phase, where the subscript l indicates a condensed phase. Taking into account a new kinetic energy of atom in vapor $\varepsilon = \varepsilon_l - \varepsilon_b$ after passing the barrier, one can obtain $d\varepsilon = mvdv = d\varepsilon_l = mv_l dv_l$, where velocities are along the x–axis. Hence, assuming the Maxwellian VDF for v_l, the evaporated atoms obtain a new VDF given by ref. 41:

$$f_x dv = \frac{Amvdv}{\sqrt{4\pi k_B T}\sqrt{\varepsilon_b + mv^2/2}} \exp\left(-\frac{\varepsilon_b + mv^2/2}{k_B T}\right), \qquad [4]$$

where a new atom velocity v is positive (i.e., directed toward the vapor) and A is a normalization factor (41). The VDFs f_y and f_z do not change during evaporation.

The above-stated simple model ignores the density redistribution and energy transfer inside the interphase boundary layer having the finite thickness, which makes a real evaporation process not as easy as it seems. Using large-scale MD simulation of nonequilibrium evaporation, we demonstrate below that evaporated atoms are released from the interphase layer almost without spending their kinetic energies, because they have a near-zero binding energy at the interphase edge. The main work required for evaporation is provided by the bulk phase, which supports via interatomic collisions a relatively slow drift of atoms through the interphase by a temperature gradient. Because the characteristic time of interatomic collisions in the condensed phase is much shorter than the drift time through the interphase (hundreds of picoseconds), the temperature remains in equilibrium

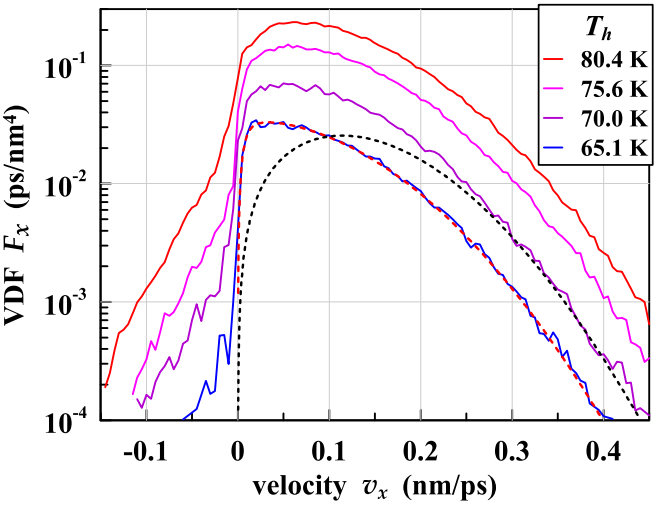

Fig. 6. VDFs in front of the absorbing boundary for different T_h. A decrease of vapor density with temperature results in a decreasing rate of interatomic collisions resulting in reduction of a backward flux. It also leads to lesser smearing of the VDF peak for small $v_x > 0$, which leads to less changes of VDF in the vapor gap for smaller T_h. The best fit (red dashed line) of VDF at $T_h = 65.1$K was obtained by Eq. 4 with $\varepsilon_b = 0.002$kJ/mol, while a model VDF (black dashed line) normalized to the same number density was built with $\varepsilon_b = 6.65$kJ/mol, which corresponds to the cohesive energy of the atom in the solid argon at $T = 65.2$K.

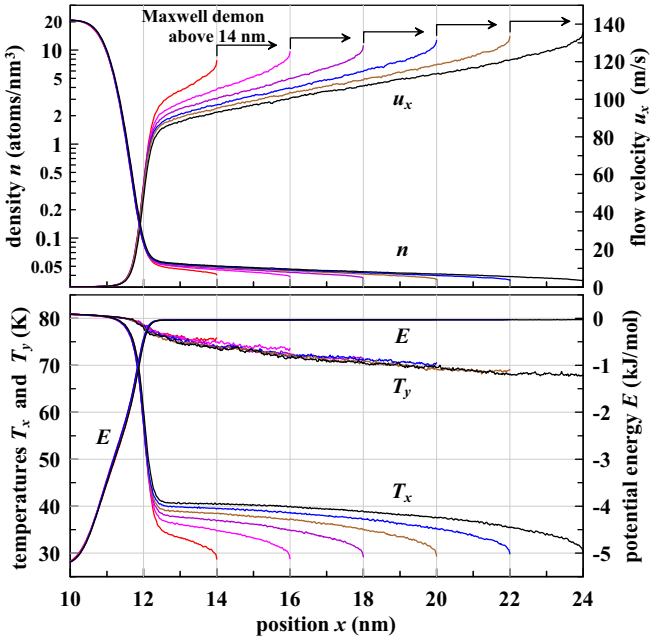

Fig. 7. Profiles of number density, temperatures, flow velocity, and averaged potential energy of atoms for different vapor gap lengths but the fixed surface temperature $T_h = 80.4$K. The absorbing boundaries with the Maxwell demons are placed at 14, 16, 18, 20, 22, and 24 nm in the MD simulation domain, which correspond to $l_{gap} = 1.5$, 3.5, 5.5, 7.5, 9.5, and 11.5 nm, respectively.

in the interphase until the density drops by one order of magnitude near the interphase edge. Thus, VDF changes gradually with decreasing density inside the interphase from a symmetrical Maxwellian form in the bulk of condensed phase to an almost semi-Maxwellian VDF for evaporated atoms, which has a form described by Eq. **4** with the binding energy $\varepsilon_b \sim 0$.

Evaporation is always associated with condensation of evaporated atoms gaining a backward velocity due to interatomic collisions in a vapor gap. Probability of such collisions increases with the length of gap l_{gap}. An additional flux j_c^- toward the hot surface is generated by evaporation from a cold surface facing the hot surface. To eliminate the flux j_c^- from the opposite cold surface and minimize the backward flux produced by collisions, we placed a nonreflective absorbing boundary on the gap l_{gap} of several nanometers from the evaporation surface. In contrast to the large vapor gap $L_{gap} = 365$nm used in the preceding and next sections, here the small vapor gaps $l_{gap} \ll L_{gap}$ are used to achieve Kn $\gg 1$ to reduce the probability of atom collisions in the gap. Such a simple approach allows us to estimate an evaporation coefficient from an intact evaporation flux undistorted by the atoms arriving to the hot surface, and those may reflect back, without monitoring of atom trajectories, which is hard to perform in the multimillion atom simulations.

The absorbing boundary is implemented with the Maxwelldemon, which watches over atom velocities in a gray zone beyond the boundary at 1.5 nm from the interphase edge, as shown in Fig. 4. If an atom gains a negative velocity v_x, the Maxwell demon subroutine replaced it by a small positive value. Atoms passing the gray zone return back to the cold side of the film like in Fig. 1; that is, Fig. 4 shows only part of the MD simulation domain to provide a better spatial resolution for density and temperature profiles in a thin interphase layer. Thus, a steady regime of evaporation, almost entirely uncoupled from condensation, is established from the hot side of film.

The interphase layer can be divided into two almost equal parts. First is the inner part between the bulk phase and a position where the temperature profile splits into the longitudinal T_x and transverse T_y temperatures, which is denoted by the left dashed line in Fig. 4. The temperature equilibrium in the inner part of interphase is well supported because the drift velocity is too small, and atoms required more than 200ps to pass this part. It is reasonable to take the position and temperature $T_h = 80.4$K at the point of temperature divergence as the surface/boundary parameters for the numerical solution of BKE.

With decreasing density by 3.5 times at the end of inner equilibrium part, the temperature T_x begins to drop, and the drift velocity is accelerated to $u_x > 0.005$nm/ps, which is recognized as a beginning of the outer nonequilibrium part of the interphase. Acceleration of mass flow to about 0.1nm/ps to the edge of this part shown by a right vertical line on Fig. 4 reduces a drift time of atoms through the outer part to about 20 ps, which is comparable with a collision time there. It leads to the large changes in VDF shape with the approach to the right edge. Fig. 5 shows VDFs constructed from velocity data accumulated in MD simulation during about 1.2ns. VDF wings with negative velocities are reduced and shrunken much in approach to the right edge of the interphase, while the width of positive VDF remains almost intact. As a result of such evolution, the longitudinal T_x drops dramatically, but the averaged kinetic energy of evaporated atoms is little affected, as it is illustrated in Fig. 4 by the longitudinal kinetic energy $K_x = \frac{m}{k_B}\langle v_x^2 \rangle$ expressed in the temperature units. The transverse $K_y = \frac{m}{2k_B}\langle v_y^2 + v_z^2 \rangle = T_y$ by definition.

The VDF marked by 0 is accumulated in a thin layer with the thickness of 0.5 nm at the end of vapor gap just before the absorbing boundary controlled by the Maxwell demon. Nevertheless, a negative velocity tail is formed here due to mostly pair collisions. Such collision conserving the total energy and P_x, P_y, and P_z momenta may result in the negative velocity of one atom along x, even though the colliding atoms have both positive velocities v_x. To get the negative atom velocity under such conditions, the required kinetic energy is redistributed from the y and z degrees of freedom of a colliding pair of atoms, which leads to a decrease of T_y seen in Fig. 4. Such collisions increase a backward flux from the absorbing boundary to the interphase edge, but the total flux remains constant everywhere. Thus, we see a larger number of atoms having negative velocities in the interphase edge VDF marked by 1 in Fig. 5.

The backward flux in vapor can be reduced by decreasing the vapor density, which can be achieved with a decreasing

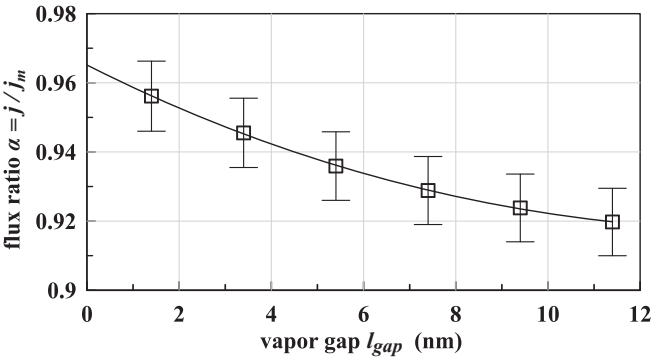

Fig. 8. Evaporation coefficient $\tilde{\alpha}(l_{gap}) = j/j_{HK}$ as a function of small vapor gap length l_{gap}. The fluxes are calculated from flow profiles presented in Fig. 7. Error bars are from uncertainty in the vapor density calculated from the red-line fit shown in Fig. 2.

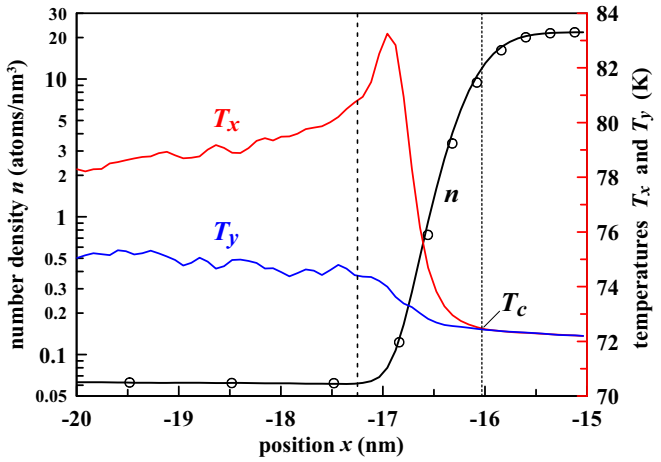

Fig. 9. Number density and temperatures profiles near a condensation surface on the cold side of liquid film shown in Fig. 1. The inner boundary of the nonequilibrium part of the interphase layer (the right dashed line) is determined by a point of divergence $T_c = 72.4$ K between longitudinal T_x and transverse T_y temperatures. The outer boundary corresponds to a point where the density profile becomes flat. Circles indicate positions where velocity data for VDFs are gathered during 1.5 ns. Evolution of instantaneous (not time-averaged) profiles is presented in Movie S1.

temperature of evaporation surface T_h. The VDFs presented on Fig. 6 were built for T_h in the range of 65.1 to 80.4 K in the systems similar to one shown on Fig. 4. The condensed phases were in solid state at 65.1 and 70 K. The Maxwell demon is always placed beyond the nonreflective absorbing boundary at the position of 14 nm, and the small vapor gaps l_{gap} vary between 1.5 and 2 nm. The collision rate drops for a larger Knudsen number at a lower density in the vapor gap, resulting in a smaller negative wing of VDF. It also prevents the large changes of VDF shape in the vapor flow from the interphase to the absorbing boundary. The lesser smearing of the VDF peak for small $v_x > 0$ for lower temperatures produces a lesser impact on the almost semi-Maxwellian VDF for atoms evaporated from the solid argon at $T_h = 65.1$K. Such VDF illustrates the idea of zero binding energy for evaporated atoms even better than VDFs obtained for higher temperatures. In these conditions, the simulated vapor flux $j \approx 1.02 j_{HK}$ for $T_h = 65.1$K is very close to the j_{HK} provided by the Hertz–Knudsen formula

$$j_{HK} = n_s \sqrt{k_B T / 2\pi m}, \qquad [5]$$

which gives the exact flux of atoms in vapor in equilibrium with a condensed phase, where a Maxwell VDF can be formally divided by two semi-Maxwellian functions at $v_x = 0$ for positive and negative fluxes, respectively.

Thus, the net evaporation coefficient defined here as $\tilde{\alpha} = j/j_{HK} \approx 1.02$ is even slightly higher than unity, which we attribute to uncertainties in the determination of surface temperature and corresponding equilibrium vapor density estimated from MD data profiles and the fit of vapor density presented in Fig. 2.

We show above that the interatomic collisions produce a backward flux in vapor, which increases with approach to the evaporation surface. To study the effect of the vapor gap length on vapor flow, we performed several MD simulations with different positions of the absorbing boundary (see Fig. 7). The higher longitudinal temperatures T_x observed in vapor for larger gap lengths are associated with the wider VDFs, which have larger wings of negative velocities produced by collisions and transported by the backward flux to an observation point from outer vapor layers. In contrast to this, the T_y profiles for the different gap lengths remain almost identical because there is no transverse flux and the energy transfer from transverse degrees of freedom to longitudinal ones depends on a local density, which does not change much. Decreasing flow velocity u_x with the gap length is also explained by the widening of the negative wings of VDFs, similarly to T_x.

Fig. 7 demonstrates that the averaged potential energy of atoms E decreases about twice in the inner part of the interphase and drops almost to zero at the end of the outer nonequilibrium part of the interface layer. Thus, the atoms releasing from the edge of interphase have a near-zero binding energy, which leads to an almost semi-Maxwellian VDF of evaporated atoms, as already demonstrated by Figs. 5 and 6. Such semi-Maxwellian VDF with $T \approx T_h$ gives the flux $j \approx j_{HK}$, which corresponds to $\alpha \approx 1$. Thus, the suggested evaporation mechanism with a near-zero binding energy yields the evaporation coefficient close to unity.

The net evaporation coefficient calculated as a function of the vapor gap length is shown in Fig. 8. It is defined as a ratio $\tilde{\alpha}(l_{gap}) = j/j_{HK}$. The evaporation coefficient as a parameter α for a numerical solution of BKE can be obtained as a limit of $\tilde{\alpha}(l_{gap}) \to \alpha$ at $l_{gap} \to 0$, at which the backward flux vanishes. It can be estimated as $\alpha \approx 0.97 \pm 0.01$. However, this formal procedure may have no physical meaning for an l_{gap} smaller than the interaction cutoff distance of 0.8125nm or the diameter 0.55nm of collision cross-section. Also, it is worth noting that another definition of temperature of evaporation surface can lead to the different vapor density n_s, which gives the different evaporation coefficient, as an example $\tilde{\alpha} \approx 0.8$ obtained in MD simulation of L–J evaporation (25).

Because the vapor fluxes calculated for temperatures in the range of 65 to 80 K are all close to j_{HK}, and due to uncertainty in the definition of the surface temperature and equilibrium vapor density, we assume that the evaporation coefficient $\alpha = 1$ for use in the numerical solution of BKE.

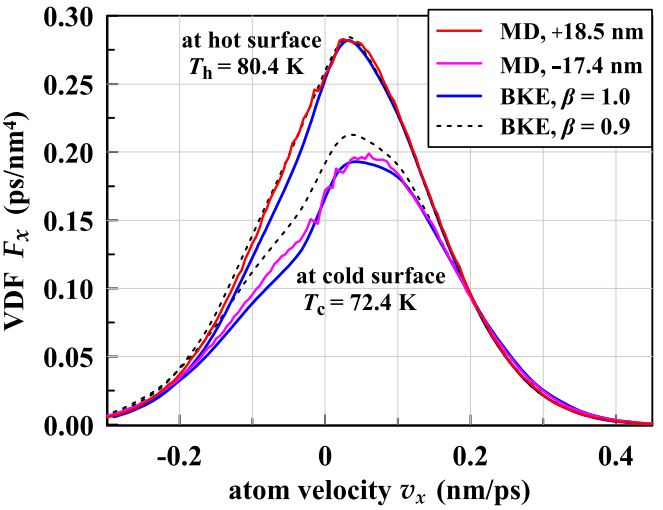

Fig. 10. VDFs obtained in MD simulation and from BKE solutions with the different condensation coefficients. VDFs are taken at the hot and cold sides of liquid film presented in Figs. 1 and 9. While the VDFs at the hot surface obtained from BKE are almost insensitive to choice of β, the VDFs at the cold surface depend strongly on this choice.

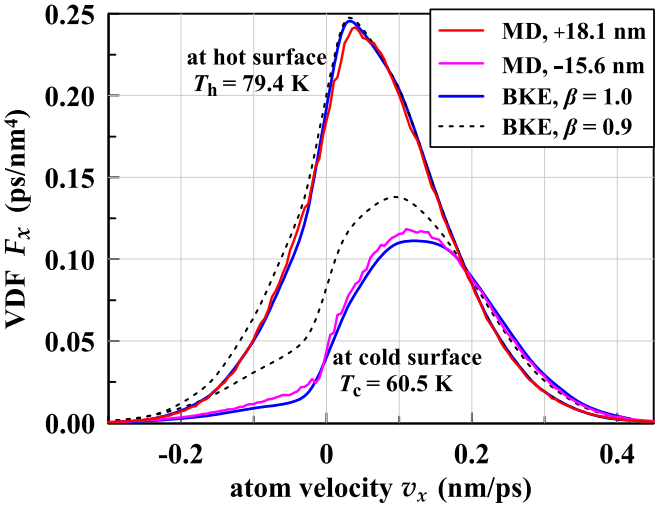

Fig. 11. VDFs obtained in MD simulation and from BKE solutions with the different condensation coefficients in evaporation–condensation between the liquid and solid sides of the same film at $T_h|T_c$ = 79.4|60.5K, respectively. Lower β results in larger negative flux from the cold surface, which leads to larger deviation from VDF provided by MD simulation.

Condensation Coefficient from Evaporation–Condensation Calculated by MD and BKE Methods

For the numerical solution of BKE in a vapor flow between the evaporation and condensation surfaces, the positions and temperatures of which are determined from MD simulation, the boundary conditions have to be imposed on VDFs on these surfaces. Assuming that the hot surface with temperature T_h is located on the left end of the gap, the positive flux j_h^+ from the surface is represented by a sum of evaporated and reflected atom fluxes. It is supposed that an atom coming to the surface with a negative flux j^- may be absorbed with probability β, which determines a condensation coefficient. Thus, the reflected atoms form the reflected flux $(1-\beta)|j^-|$, which together with the evaporated atom flux expressed as αj_{HK} using Eq. **5** results in the positive flux $j_h^+ = \alpha j_{HK} + (1-\beta)|j^-|$. The required boundary VDF must yield this flux.

As we demonstrated in *Evaporation Coefficient from MD Simulation*, the VDF of evaporated atoms is represented by the semi-Maxwellian VDF $f_{HK}(T_h)$ for T_h, which yields the Hertz–Knudsen flux. The VDF of reflected atoms can also be represented by a similar semi-Maxwellian function $\sim f_{HK}$, because the reflection is assumed to be diffuse with perfect accommodation to the surface temperature. To produce the reflected flux, the VDF f_{HK} must be normalized by the j_{HK} and multiplied by the $(1-\beta)|j^-|$. Therefore, the left boundary condition applied for a positive wing of VDF at the surface is given by

$$f_h^+ = (\alpha + (1-\beta)|j^-|/j_{HK}) f_{HK}(T_h) = \tilde{\alpha} f_{HK}(T_h). \quad [6]$$

The negative wing βf^- is eliminated on the left boundary.

Similarly, the right boundary condition imposed on the cold surface at T_c is given by

$$f_c^- = (\alpha + (1-\beta)|j^+|/j_{HK}) f_{HK}(T_c), \quad [7]$$

where we assume that the α is equal to that on the hot surface. As indicated in *Evaporation Coefficient from MD Simulation*, the evaporation coefficient is almost independent of temperature, and $\alpha \approx 1$ in MD simulation of evaporation; hence, $\alpha = 1$ is applied on both boundaries in BKE calculations. The unknown condensation coefficient β is also taken to be independent of surface temperature.

Definition of position and temperature of the cold surface is similar to that for the hot surface introduced in the discussion of Fig. 4. The density and temperature profiles with a point of divergence between the longitudinal T_x and transverse T_y temperatures on the cold side of the film presented in Fig. 1 in the vicinity of the interphase layer are shown in Fig. 9. Thus, the position and temperature of the right boundary used in BKE calculations are determined at the end of the equilibrium part of the cold interphase layer formed in MD simulation of steady evaporation–condensation.

By varying the β, governing both boundary conditions in Eqs. **6** and **7**, the VDFs obtained by MD and BKE methods can be compared with the aim to find an optimal condensation coefficient leading to a good agreement between those VDFs. We find numerical solutions of BKE with $\beta = 0.8; 0.9; 1$ for two evaporation–condensation systems with $T_h|T_c$ = 80.4|72.4K in the vapor gap L_{gap} = 364.3nm and $T_h|T_c$ = 79.4|60.5K in the vapor gap L_{gap} = 366.7nm. See details of simulations in *SI Appendix*. Fig. 10 shows the VDFs taken at hot and cold surfaces of liquid film for $\beta = 0.9; 1$. The VDFs for $\beta = 0.8$ are not shown because they give the largest deviation from the VDFs obtained in MD. One can see that the VDFs from BKE are weakly dependent on β at the hot surface, while BKE solution at the cold surface is very sensitive to the variation of β.

Similar VDFs from BKE solutions of evaporation–condensation between the liquid and solid sides of the same film at $T_h|T_c$ = 79.4|60.5K, respectively, are shown in Fig. 11. The corresponding flow profiles are presented in Fig. S2. The steady regime of vapor flow in the corresponding MD simulation is illustrated in Movies S1 and S2, where the instantaneous (not time-averaged) profiles of density and temperatures across the cold and hot interphase layers are shown, respectively. The density profile is almost static, and only temperatures in the low-dense vapor experience the natural fluctuations in those videos. It is readily seen that the point of temperature divergence appears at very low number density within the interphase layer, which implies the fast energy exchange between atoms there, as discussed in *Evaporation Coefficient from MD Simulation*. Fig. 11 shows again that the VDF on the hot surface is almost insensitive to the choice of β.

Thus, β as a fitting parameter is determined primarily by the VDF at the cold surface. Lower β produces a larger vapor flux from the condensation surface, which must be compensated by a positive flux to the surface since the total flux in the steady evaporation–condensation is fixed. As a result, the number density at the cold surface becomes higher than this in MD simulation.

The above comparison of VDFs from MD simulations and solutions of BKE indicates that the best condensation coefficient is $\beta = 1$ in the considered temperature range. The best agreement between the flow profiles obtained in MD and BKE calculations is also achieved at $\beta = 1$, as illustrated in Figs. S3 and S4.

SI Appendix provides the detailed description of the simulation technique and comparison of MD and BKE temperature profiles. Movies S1 and S2 show snapshots of density and temperature profiles across the interphase layer on the condensation side for $T_c|T_h$ = 72.4|80.4K and on the evaporation side for $T_h|T_c$ = 79.4|60.5K, respectively.

Conclusions

Consistent application of MD and BKE methods to the problem of evaporation–condensation bridges the gap between the atomistic representation of complex atom motion and probabilistic evolution of velocity distributions between two surfaces of the condensed material. Using multimillion atom simulation, we demonstrate that, contrary to intuition, atoms are released from a condensed phase without the use of their kinetic energy but with the support from collisions with other atoms in the interphase layer. This effectively means that the evaporated atoms have a near-zero binding energy, which leads to the virtually semi-Maxwellian VDF of evaporated atoms and evaporation coefficient close to unity.

We also find that the best agreement between the steady flow profile and VDFs obtained by MD and BKE methods is achieved if both evaporation and condensation coefficients are close to unity in the considered conditions.

We think that the evaporation–condensation of liquid metals, water, and polyatomic molecular liquids should be studied next to verify the applicability of our results to more complex materials. Such studies may provide more appropriate boundary conditions for use in continuum mechanics approaches to the evaporation–condensation problem.

Acknowledgments

This work was supported by Russian Foundation for Basic Research Grant 17-08-00805. S.I.A. was supported by Russian Science Foundation Grant 14-19-01599.

1 Kozyrev AV, Sitnikov AG (2001) Evaporation of a spherical droplet in a moderate-pressure gas. *Phys Usp* 44:725–733.
2 Maxwell JC (1890) *The Scientific Papers of James Clerk Maxwell*, ed Niven WD (Cambridge Univ Press, Cambridge, UK), Vol 2.
3 Langmuir I (1915) The dissociation of hydrogen into atoms. [Part II] Calculation of the degree of dissociation and the heat of formation. *J Am Chem Soc* 37:417–458.
4 Hertz H (1882) Ueber die verdunstung der Flüssigkeiten, insbesondere des quecksilbers, im luftleeren raume. *Ann Phys* 253:177–193.
5 Knudsen M (1915) Die maximale verdampfungsgeschwindigkeit des quecksilbers. *Ann Phys* 352:697–708.
6 Kucherov RY, Rikenglaz LE (1960) On hydrodynamic boundary conditions for evaporation and condensation. *Sov Phys JETP* 37:88–89.
7 Labuntsov DA (1967) An analysis of the processes of evaporation and condensation. *High Temp* 5:579–647.
8 Muratova TM, Labuntsov DA (1969) Kinetic analysis of the processes of evaporation and condensation. *High Temp* 7:959–967.
9 Kogan MN, Makashev NK (1971) Role of the Knudsen layer in the theory of heterogeneous reactions and in flows with surface reactions. *Fluid Dyn* 6:913–920.
10 Pao Y-P (1971) Application of kinetic theory to the problem of evaporation and condensation. *Phys Fluids* 14:306–312.
11 Yen SM (1973) Numerical solutions of non-linear kinetic equations for a one-dimensional evaporation-condensation problem. *Comput Fluids* 1:367–377.
12 Fischer J (1976) Distribution of pure vapor between two parallel plates under the influence of strong evaporation and condensation. *Phys Fluids* 19:1305–1311.
13 Aoki K, Cercignani C (1983) Evaporation and condensation on two parallel plates at finite Reynolds numbers. *Phys Fluids* 26:1163–1164.
14 Cercignani C, Fiszdon W, Frezzotti A (1985) The paradox of the inverted temperature profiles between an evaporating and a condensing surface. *Phys Fluids* 28:3237–3240.
15 Hermans LJF, Beenakker JJM (1986) The temperature paradox in the kinetic theory of evaporation. *Phys Fluids* 29:4231–4232.
16 Koffman LD, Plesset MS, Lees L (1984) Theory of evaporation and condensation. *Phys Fluids* 27:876–880.
17 Anisimov SI (1968) Vaporization of metal absorbing laser radiation. *Sov Phys JETP* 27:182–183.
18 Anisimov SI, Imas YA, Romanov GS, Khodyko YV (1971) Effects of High-Power Radiation on Metals (Joint Publications Research Service, Washington, DC).
19 Anisimov SI, Rakhmatulina AK (1973) The dynamics of the expansion of a vapor when evaporated into a vacuum. *Sov Phys JETP* 37:441–444.
20 Tcheremissine FG (2006) Solution to the Boltzmann kinetic equation for high-speed flows. *Comput Math Math Phys* 46:315–329.
21 Aristov VV (2001) *Direct Methods for Solving the Boltzmann Equation and Study of Nonequilibrium Flows*. Fluid Mechanics and its Applications, ed Moreau R (Springer, Dordrecht, The Netherlands), Vol 60.
22 Kryukov A, Levashov V, Shishkova I (2001) Numerical analysis of strong evaporation–condensation through the porous matter. *Int J Heat Mass Transfer* 44:4119–4125.
23 Kryukov AP, et al. (2006) Selective water vapor cryopumping through argon. *J Vac Sci Technol A* 24:1592–1596.
24 Kryukov A, Levashov V, Shishkova I (2009) Evaporation in mixture of vapor and gas mixture. *Int J Heat Mass Transfer* 52:5585–5590.
25 Zhakhovskii V, Anisimov S (1997) Molecular-dynamics simulation of evaporation of a liquid. *J Exp Theor Phys* 84:734–745.
26 Marek R, Straub J (2001) Analysis of the evaporation coefficient and the condensation coefficient of water. *Int J Heat Mass Transfer* 44:39–53.
27 Ishiyama T, Fujikawa S, Kurz T, Lauterborn W (2013) Nonequilibrium kinetic boundary condition at the vapor-liquid interface of argon. *Phys Rev E* 88:042406.
28 Kon M, Kobayashi K, Watanabe M (2016) Liquid temperature dependence of kinetic boundary condition at vapor–liquid interface. *Int J Heat Mass Transfer* 99:317–326.
29 Meland R, Ytrehus T (2007) Molecular dynamics simulation of evaporation of two-component liquid. *Proceedings of 25th International Symposium on Rarefied Gas Dynamics*, eds Ivanov MS, Rebrov AK (Publ. House of the Siberian Branch of the Russian Acad. of Sciences, Novosibirsk), pp 1229–1232.
30 Yang T, Pan C (2005) Molecular dynamics simulation of a thin water layer evaporation and evaporation coefficient. *Int J Heat Mass Transfer* 48:3516–3526.
31 Cheng S, Lechman JB, Plimpton SJ, Grest GS (2011) Evaporation of Lennard-Jones fluids. *J Chem Phys* 134:224704.
32 Kon M, Kobayashi K, Watanabe M (2014) Method of determining kinetic boundary conditions in net evaporation/condensation. *Phys Fluids* 26:072003.
33 Kon M, Kobayashi K, Watanabe M (2017) Kinetic boundary condition in vapor-liquid two-phase system during unsteady net evaporation/condensation. *Eur J Mech B Fluids* 64:81–92.
34 Kobayashi K, Sasaki K, Kon M, Fujii H, Watanabe M (2017) Kinetic boundary conditions for vapor–gas binary mixture. *Microfluid Nanofluid* 21:53.
35 Kobayashi K, Hori K, Kon M, Sasaki K, Watanabe M (2016) Molecular dynamics study on evaporation and reflection of monatomic molecules to construct kinetic boundary condition in vapor–liquid equilibria. *Heat Mass Transfer* 52:1851–1859.
36 Kogan MN (1969) Rarefield Gas Dynamics (Plenum, New York).
37 Heerman DW (1986) Computer Simulation Methods in Theoretical Physics (Springer, Berlin).
38 Haynes WM, ed (2017) CRC Handbook of Chemistry and Physics (CRC Press, Boca Raton, FL), 97th Ed, pp 6-128 and 15-10.
39 Zhakhovskii VV, Zybin SV, Nishihara K, Anisimov SI (1999) Shock wave structure in Lennard-Jones crystal via molecular dynamics. *Phys Rev Lett* 83:1175–1178.
40 Shishkova IN, Sazhin SS (2006) A numerical algorithm for kinetic modelling of evaporation processes. *J Comput Phys* 218:635–653.
41 Gerasimov DN, Yurin EI (2014) The atom velocity distribution function in the process of liquid evaporation. *High Temp* 52:366–373.